



# Synthesis, characterizations and single crystal structure of di-nuclear azido-bridged Cd(II) coordination polymer with Schiff base precursor ( $H_2L_{\text{pent}}^{\text{OMe}}$ ): DFT, fluorescence, solvatochromism and *in vitro* antimicrobial assay



Dhrubajyoti Majumdar<sup>a,b</sup>, Dhiraj Das<sup>c</sup>, S.S. Sreejith<sup>d</sup>, Sudip Nag<sup>e</sup>, Swapan Dey<sup>b,\*</sup>, Surajit Mondal<sup>b</sup>, Kalipada Bankura<sup>a</sup>, Dipankar Mishra<sup>a,\*</sup>

<sup>a</sup> Department of Chemistry, Tamralipta Mahavidyalaya, Tamluk 721636, West Bengal, India

<sup>b</sup> Department of Applied Chemistry, Indian Institute of Technology (Indian School of Mines), Dhanbad, Jharkhand 826004, India

<sup>c</sup> Department of Chemical Sciences, IISER, Mohali, Manauli, PO 140306, India

<sup>d</sup> Department of Applied Chemistry, Cochin University of Science and Technology, Kochi 682022, Kerala, India

<sup>e</sup> Department of Biochemistry, University of Calcutta, 35 Ballygunge Circular Road, Kolkata 700019, India

## ARTICLE INFO

### Keywords:

Azide  
Antibacterial  
Cd(II)  
DFT  
Schiff base  
Solvatochromism  
Fluorescence

## ABSTRACT

A di-nuclear azido-bridged Cd(II) 1-D coordination polymer  $[Cd_2(H_2L_{\text{pent}}^{\text{OMe}})(\mu_{1,1}-N_3)_2]_n$  (**1**) has been successfully synthesized using less explored bi-compartmental Schiff base ligand ( $H_2L_{\text{pent}}^{\text{OMe}}$ ) and characterized by elemental analysis, FT-IR, FT-Raman, UV-Visible, SEM-EDAX, powder X-ray diffraction and fluorescence spectroscopy. Solid-state X-ray single crystal study revealed two different geometrical environment of Cd metal centres with distorted square pyramidal (Cd1) and distorted pentagonal bipyramid (Cd2). Overall, small-sized azide ions in asymmetric unit act as  $\mu_{1,1}$  bridging mode. Geometry is optimized in gas phase using ORCA 3.0.3 and B3LYP level TZVP basis set to explain frontier molecular orbitals (FMO), molecular electrostatic potential (MEP) and global reactivity. The HOMO-LUMO energy gap (3.434 eV) suggests that chemical reactivity of complex **1** is low but fairly stable. Moreover, molecular electrostatic potential map was drawn to identify reactive regions in terms of electrophilic and nucleophilic. The steady state and time-resolved fluorescence properties have been explored in DCM and solid-state condition at room temperature. Complex **1** exhibit bi and tri-exponential decay in DCM as well as solid-state. The fluorescence behaviours are predominantly intra-ligand in nature ( $\pi \rightarrow \pi^*$ ) with lifetimes in the range (1.16–1.11 ns). Solvatochromism has been reported to show solvent dependent absorption and fluorescence spectral changes. Fascinatingly, red shifted solvatochromism was observed upon increasing solvent polarity. Finally, concentration dependent antimicrobial activity was investigated against two standard bacterial strains (*Staphylococcus aureus* (ATCC 25923) and Methicillin-resistant *Staphylococcus aureus* (MRSA) where 250 µg/ml concentration of complex **1** is sufficient to show the antimicrobial effect.

## 1. Introduction

Today in modern scientific society application-based research works gaining much more importance due to invention of human helpful materials and saving environment from accidental disaster. In this juncture, branch of materials science claims to be an active participant for scientific revolution after gatherings physics, chemistry and biology under single umbrella. The coordination polymers (CPs)/MOFs belongs one of the active members in material science [1]. CPs are referred as

active hybrid compounds composed of organic and inorganic materials. Herein we observed Schiff bases in conjunction with pseudo-halide anions donor centres act as spacer and metal ions as active metal nodes [2]. Thus, in the last two decades, conception of CPs/MOFs and poly-nuclear discrete complexes has been expanded dramatically in presence of well-known pseudo-halide ions such as  $N_3^-$ ,  $NCS^-$ ,  $OCN^-$ ,  $[N(CN)_2^-]$  [3–24] along with aromatic benzene, heterocyclic-multicarboxylic compounds, oxalate, squarate and croconate dianions [25–29]. These pseudo-halide ions effectively bind different metal ions to isolate large

\* Corresponding authors.

E-mail addresses: [deyswapan77@yahoo.com](mailto:deyswapan77@yahoo.com) (S. Dey), [dmishra.ic@gmail.com](mailto:dmishra.ic@gmail.com) (D. Mishra).

number of coordination complexes which have interesting molecular and crystalline architectures with different dimensionality [3–29]. Among these, small-sized pseudo-halide azide ions is a nice linker since it can bridge metal ions in many different coordination bonding modes [4–22,30]. Although several azido-bridged CPs/MOFs have been previously reported but formation of M(II)-azido Schiff base complexes always deserves new insights of research in respect novel structure formation [31] and have broad spectrum of properties such as gas adsorption and separation [32], ion exchange [33], sensing [31], luminescence [34], antibacterial and anti-biofilm [35]. In fact, research of azido-bridged complexes with paramagnetic centre metal ions have been subjected to extensive studies in connection of magnetic exchange interaction whereas Schiff base complexes derived from d<sup>10</sup> metal ions did not receive such attention [4–22,30].

Due to our long-standing interest in *ortho*-vanillin derived bi-compartmental Schiff base ligands, till date we have explored such ligand complexation with d<sup>10</sup> metal ions and their associated photoluminescence, DFT, *in vitro* antibacterial and anti-biofilm properties vividly [36]. The outcome of previous research works is that azido-bridged complexes exhibit photophysical, antibacterial and anti-biofilm properties [35] but no exiguous number of studies on the concentration dependent *in vitro* antimicrobial activity against two standard bacterial strains (*Staphylococcus aureus* (ATCC 25923) and Methicillin-resistant *Staphylococcus aureus* (MRSA). Unlike other metals, Cd(II) is well-known to exhibit flexible geometry owing to its d<sup>10</sup> electronic configuration and zero crystal field stabilization energy (CFSE). The geometry of cadmium metal ion is primarily controlled by the steric requirements of the Schiff base ligands [37]. Schiff base ligands based on o-vanillin condensed with 1,3-diaminopentane are scarce in literature [37]. Further, since Schiff base ligands gaining day to day popularity in coordination chemistry domain, researchers around the world have been recommended such unique ligands for synthetic aspect of M(II)-complexes due to their preoperational accessibilities, structural varieties, extreme stability, plasticity, varied dentencies [38]. In fact, herein tuning of bi-compartmental Schiff base (H<sub>2</sub>L<sub>pent</sub><sup>OMe</sup>) is to search if any important changes occur in the molecular and crystalline architectures, complex dimensionality and biological interest.

In this paper, we have reported synthetic details, characterisations, SEM-EDAX, solid-state single crystal structure, DFT, solvatochromism, fluorescence and *in vitro* concentration dependent antimicrobial activity of one new Cd(II) CP viz., [Cd<sub>2</sub>(H<sub>2</sub>L<sub>pent</sub><sup>OMe</sup>)<sub>2</sub>(μ<sub>1,1</sub>-N<sub>3</sub>)<sub>2</sub>]<sub>n</sub> (**1**).

## 2. Experimental section

### 2.1. Materials and physical measurements

The research chemicals were of analytical grade and used as purchased without further purification. o-vanillin and 1,3-diaminopentane was purchased from Sigma Aldrich Company, USA. Cd(OAc)<sub>2</sub>·2H<sub>2</sub>O and sodium azide (NaN<sub>3</sub>) was purchased from E. Merck, SDFCL, India. Elemental analysis was performed on a Perkin-Elmer 2400 elemental analyzer. FT-IR and FT-Raman spectra were recorded as KBr pellets (4000–400 cm<sup>-1</sup>) using Perkin-Elmer spectrum RX 1 and BRUKER RFS 27 (4000–50 cm<sup>-1</sup>). EDAX experiments for weight percentage (%) analysis of different elements was performed on EDAX OXFORD XMX N using Tungsten filament. SEM images analysed by JEOL Model JSM – 6390LV. UV-Visible spectra (200–1100 nm) were determined by using Hitachi model U-3501 spectrophotometer. Fluorescence spectra (spectroscopic grade DCM solvent) were measured by using Perkin-Elmer LS50B Spectrofluorometer model at room temperature. Fluorescence lifetime measurements were recorded using JOBIN-VYON M/S Fluorimeter. Fluorescence lifetime (RT) in DCM solvent and solid-state is calculated using Equation S1. Powder X-ray diffraction measurements were carried out using BRUKER AXS, GERMANY X-ray diffractometer model using radiation Cu Kα-1. Quantum yield (Φ) for **1** was determined by applying Eq. (1) where quinine sulphate is preferentially

used as secondary standard (Φ = 0.57 in water) [39]

$$\frac{\Phi_S}{\Phi_R} = \frac{A_S}{A_R} \times \frac{(Abs)_R}{(Abs)_S} \times \frac{n_S^2}{n_R^2} \quad (1)$$

From Eq. (1) A terms denote the fluorescence area under the curve; Abs denotes absorbance; n is the refractive index of the medium; Φ is the fluorescence quantum yield; and subscripts S and R denote parameters for the studied sample and reference compound respectively.

### 2.2. X-ray crystallography

Good quality crystal data for cadmium complex was collected on a Bruker SMART CCD [40] diffractometer using Mo K<sub>α</sub> radiation at λ = 0.71073 Å. For data collection purpose different well-known programs were operated e.g. SMART program used for collecting frames of data, indexing reflections and determining lattice parameters, SAINT [41] for integration of the intensity of reflections and scaling, SADAB [42] for absorption correction and popular SHELXTL for space group, structure determination and least-squares refinements on F<sup>2</sup>. Crystal structure was fully solved after refining by full-matrix least-squares methods against F<sup>2</sup> using the common program SHELXL-2014 [43] and Olex-2 software [44]. It is worth mentioning that the Alert level A in the checkCIF1 is related only to the Rint value is greater than 0.25 and 0.12 since the examined single crystal was a small-sized, brittle and weakly diffracting (despite using Mo K<sub>α</sub> radiation). Multiple attempts were made to grow better quality diffracting crystal. The data here reported is the best one among the collected. All the non-hydrogen atoms were refined with anisotropic displacement parameters and hydrogen positions were fixed at calculated positions which is refined isotropically. All crystallographic figures for complex **1** were constructed using latest Diamond software [45]. The crystallographic data and full structure refinement parameters are shown in Table 1. Crystallographic data (excluding structure factors) have been deposited with the Cambridge Crystallographic Data Centre as supplementary publication number CCDC 1915504. Copies of the data can be obtained, free of charge, on

**Table 1**  
Crystal structure parameters for complex **1**.

Formula	C <sub>21</sub> H <sub>24</sub> Cd <sub>2</sub> N <sub>8</sub> O <sub>4</sub>
M/g	677.28
Crystal system	Monoclinic
Space group	C2/c
a/Å	21.811(2)
b/Å	12.5480(13)
c/Å	19.0299(19)
α (°)	90
β (°)	107.288(6)
γ (°)	90
V/Å <sup>3</sup>	4972.9(9)
Z	8
ρ <sub>e</sub> /g cm <sup>-3</sup>	1.809
μ/mm <sup>-1</sup>	1.754
F(0 0 0)	2672
Cryst size (mm <sup>3</sup> )	0.2 × 0.2 × 0.1
θ range (deg)	0.996
Limiting indices	-25 ≤ h ≤ 25 -14 ≤ k ≤ 14 -21 ≤ l ≤ 22
Refns collected	23,745
Ind reflns	4119 [R <sub>int</sub> = 0.4422, R <sub>sigma</sub> = 0.3375]
Completeness to θ (%)	0.996
Refinement method	Full-matrix-block least-squares on F <sup>2</sup>
Data/restraints/ parameters	4119/0/313
Goodness-of-fit on F <sup>2</sup>	0.941
Final R indices [I greater than 2σ(I)]	R <sub>1</sub> = 0.0805 wR <sub>2</sub> = 0.0627
R indices (all data)	R <sub>1</sub> = 0.2469 wR <sub>2</sub> = 0.0804
Largest diff. peak and hole (e · Å <sup>-3</sup> )	0.575 and -0.505

application to CCDC, 12 Union Road, Cambridge CB2 1EZ, U.K.: <http://www.ccdc.cam.ac.uk/cgi-bin/catreq.cgi>, e-mail: data\_request@ccdc.cam.ac.uk, or fax: +44 1223 336033.

### 2.3. Computational methodologies

The initial structure for the DFT calculations were taken from the single crystal structure (cif 1) of the crystallographic coordinates of the compound. Gas phase optimization of the title complex was done using ORCA 3.0.3 software [46]. Frequency calculations were done to confirm that the optimized structure is the global minima and calculations returned no imaginary frequency. The Becke's three-parameter hybrid exchange functional including the Lee-Yang-Parr nonlocal correlation functional (B3LYP) [47] and the triple zeta valence basis set with one set of polarization function (TZVP) [48] was used. To accelerate the calculations, we utilized the resolution of identity (RI) approximation with the decontracted auxiliary def2-TZV/J Coulomb fitting basis sets and the chain-of-spheres (RIJCOSX) approximation to exact exchange as implemented in ORCA [49]. The choice of the TZVP basis set was made on the known fact that it reduces the basis set superposition error (BSSE) to negligible in the calculation of systems with non-covalent interactions. The optimized structure of complex 1 was used to find out electrostatic potential regions. The visualization of the frontier orbitals was done using Avogadro software [50]. Orbital contribution analysis of the frontier orbitals is carried out using Mulliken method by employing Multiwfn software [51].

### 2.4. Experimental of antimicrobial assay

The antimicrobial efficiency of complex 1 was tested against the test organism *Staphylococcus aureus* (ATCC 25923) and Methicillin-resistant *Staphylococcus aureus* (MRSA). The quantitative analysis was studied by cell viability assay [51]. Briefly, the bacterial cells were cultured in Luria Bertini (LB) broth in 96 well plate. Different concentration (250, 500 and 1000 µg/ml) of complex 1 were added in well containing bacterial culture and incubated for 24 hrs. Here, gentamicin solution (10 µg/ml) was utilized as a positive control. The antimicrobial efficiency was investigated by measuring optical density of cells using microplate reader (Biorad, USA) at 600 nm compared to control. Cell viability was determined using the given well-known formula:

$$\text{CellViability}(\%) = \frac{\text{OD}_{\text{Sample}} - \text{OD}_{\text{Blank}}}{\text{OD}_{\text{Control}} - \text{OD}_{\text{Blank}}} \times 100$$

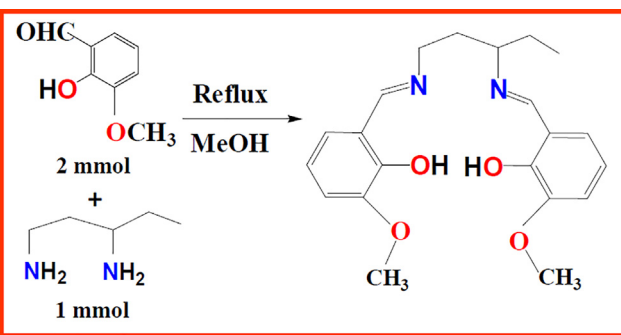
The absorbance values of treated cells and untreated cells are denoted as  $\text{OD}_{\text{Sample}}$  and  $\text{OD}_{\text{Control}}$  respectively. The whole assay was performed with independent triplicate experimental setup to obtain the standard mean values.

### 2.5. Synthesis of ligand ( $H_2L_{\text{pent}}^{\text{OMe}}$ )

Schiff base ligand ( $H_2L_{\text{pent}}^{\text{OMe}}$ ) was synthesized using a reported procedure [52]. Briefly, using the condensation process of 1 mmol o-vanillin (3-methoxysalicylaldehyde) (0.152 g) with 0.5 mmol (0.0511 g) 1,3-diaminopentane in (25 mL) of methanol for ca. 3 h (Scheme 1). The yellow solution was used for complex 1 formation.

### 2.6. Synthesis of $[Cd_2(H_2L_{\text{pent}}^{\text{OMe}})(\mu_{1,1}-N_3)_2]_n$ (1)

To a methanol solution (25 mL) of cadmium acetate dihydrate (0.266 g, 1 mmol), a yellow solution of Schiff base ligand was slowly added followed by sodium azide (0.065 g, 1 mmol) in minimum volume of aqueous methanol with constant stirring for 2.5 h. 5–6 drops of DCM were then added and the resulting mixture was additionally refluxed for 1 h at 75 °C. Finally, yellow filtrate was kept in refrigerator for crystallization by slow evaporation. After 5 days light yellow coloured single crystal suitable for X-ray crystallography was obtained. Crystals were isolated by filtration and air-dried. Yield: 0.455 g, Anal. Calc. for



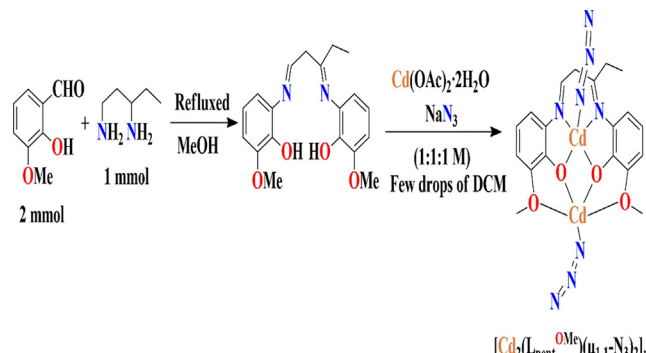
**Scheme 1.** Synthetic Scheme for Schiff base ligand.

$C_{21}H_{24}N_8O_4Cd_2$ : C, 37.24; H, 3.57; N, 16.54. Found: C, 37.18; H, 3.48; N, 16.34%. IR (KBr  $\text{cm}^{-1}$ ) selected bands:  $\nu$  2965 (w), 2852 (w), 2074 (vs), 2049 (vs), 1622 (vs), 1469 (s), 1213 (s), FT-Raman ( $\text{cm}^{-1}$ ) selected bands: 2987 (w), 2929 (s), 2085 (s), 1632 (vs), 1457 (s), 1217 (w), UV-Vis  $\lambda_{\text{max}}$  (DCM): 353 nm.

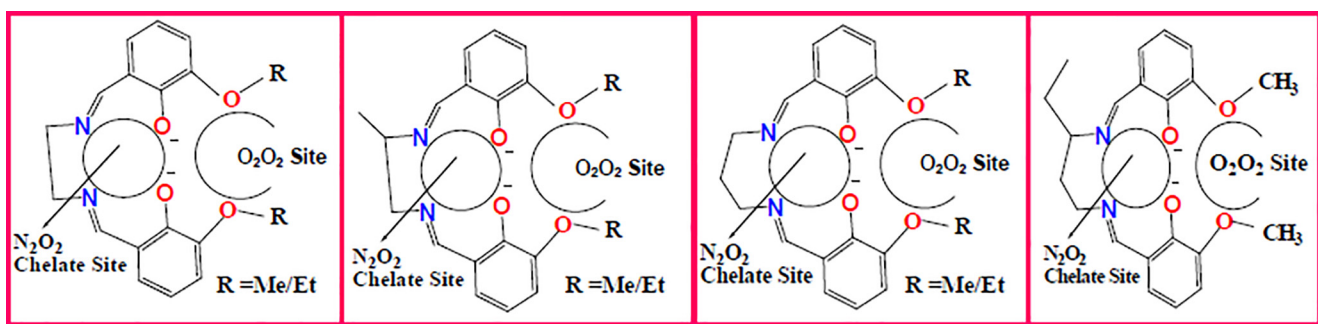
## 3. Results and discussion

### 3.1. Synthesis

( $H_2L_{\text{pent}}^{\text{OMe}}$ ) was synthesized by the condensation of 1,3-diaminopentane with o-vanillin in MeOH at 1:2 M ratio [52]. Complex 1 derived from o-vanillin condensed Schiff base ( $H_2L_{\text{pent}}^{\text{OMe}}$ ) was prepared in moderate good yield by taking the following procedure where 1:1:1 M ratio of cadmium acetate dihydrate, ( $H_2L_{\text{pent}}^{\text{OMe}}$ ) and sodium azide in methanolic solution under stirred condition (Scheme 2). Di-nuclear azido-bridged cadmium complex was isolated only from slow evaporation of (CH<sub>3</sub>OH-DCM). Salicylaldehyde derivatives are always useful carbonyl precursor for syntheses of large variety of Schiff base ligands since additional coordinating group (-OR, R = Me, Et) enhanced not only ligand denticity but accelerated the possibility of CPs/polynuclear complex formation [53]. The versatile bridging nature of ( $H_2L_{\text{pent}}^{\text{OMe}}$ ) and azide ions are nicely presented in Scheme S1-S2. Ligand structure comprises two imines, two phenols and one (-OR, R = Me) group. After de-protonation, the N<sub>2</sub>O<sub>2</sub> imine-based chelating site has the effective binding property with M<sup>2+</sup> metal ions (Scheme 3). In fact, CPs formation with Cd(II)-node and azide ions are scarce in literature. Furthermore, ligand structural framework opens up similarities with other bi-compartmental ligands (Scheme 3) [35,36,54]. In this context, our research team extended the coordination behaviour of ( $H_2L_{\text{pent}}^{\text{OMe}}$ ) with Cd(II) and small-sized azide ions (Table 2). The stoichiometry of 1 was corroborated by the microanalytical results and successfully characterized by FT-IR, FT-Raman, UV-Vis, SEM-EDAX, powder X-ray diffraction, X-ray crystallography and fluorescence spectroscopy.



**Scheme 2.** Synthetic scheme for complex 1.

Scheme 3. Similarities of ligand ( $H_2L_{\text{pent}}^{\text{OMe}}$ ) with other compartmental ligands.

### 3.2. Spectral characterizations

Di-nuclear complex formation was characterized by (ATR-FT-IR, FT-Raman and UV-Vis) spectroscopic methods (Fig. S1, Fig. S2, Fig. S3). The characteristic imines ( $\text{C}=\text{N}$ ) stretching vibration Schiff base ligand was found to be  $1629 \text{ cm}^{-1}$  [52]. The absence of the  $\text{N}-\text{H}$  stretching band near at  $3150 \text{ cm}^{-1}$  positively confirmed the condensation of all the primary amine groups [52]. Stretching band at  $3449 \text{ cm}^{-1}$  of Schiff base is due to  $\text{O}-\text{H}$  stretching which completely disappeared in 1. In 1, FT-IR and FT-Raman ( $\text{C}=\text{N}$ ) stretching vibration bands are shifted to  $1622 \text{ cm}^{-1}$  (for IR) (Fig. S1) and  $1632 \text{ cm}^{-1}$  (for Raman) respectively (Fig. S3). These spectroscopic data confirmed the coordination mode of the imine nitrogen atom to the cadmium metal centre [55]. 1 exhibit strong bands near at  $2049$ ,  $2074$  (for FT-IR) and  $2085 \text{ cm}^{-1}$  (for FT-Raman) [56] attributable to  $\nu(\text{N}_3)$  binding (Fig. S1 and Fig. S3). Additionally, aliphatic  $\text{C}-\text{H}$  stretching resonance for 1 observed near at  $2965 \text{ cm}^{-1}$  (for FT-IR) and  $2987 \text{ cm}^{-1}$  (for FT-Raman) respectively. Ar-O stretching frequency observed at  $1213 \text{ cm}^{-1}$  (for FT-IR) and  $1217 \text{ cm}^{-1}$  (for FT-Raman) which is identical with previously reported other salen ligands [57]. Therefore, IR and Raman spectroscopic investigations gives clear conclusive idea of azido ions bridging propensity. Moreover, IR spectral data of  $\text{Cd}_2$ -nuclear metal complex were thoroughly compared with previously reported  $\text{Cd}(\text{II})$ -azido complexes (Table S2).

### 3.3. EDAX-SEM

The weight (%) contribution of the elements in  $\text{Cd}_2$ -nuclear metal complex was confirmed from EDAX analysis (Table S3) and the related EDAX profile in Fig. S4. The calculated and EDAX values of complex 1 are nearly in good agreement. Therefore, the empirical formula of 1 is formulated as  $\text{C}_{21}\text{H}_{24}\text{N}_8\text{O}_4\text{Cd}_2$ . The EDAX spectrum shows the peaks of highest for C and thereafter O, Cd which further supported the empirical formula of 1. The important structural morphological features of 1 is also supported by SEM (scanning electron microscope) images (Fig. 1). SEM images characterized size and morphological structure [58].

SEM images are produced with different concentrations for complex 1 (Fig. 1) and images does not indicate the presence of well-defined crystals free from any shadow of the metal ion on the surface. It is seen clearly from SEM images that complex 1 exhibit platelet-like structures

[58]. The particle size is in the diameter range of few microns. In terms of Fig. 4 very good quality grain images for 1 are obtained until 1-2-1  $\mu\text{m}$  growth rate. SEM images grain size maximum at  $1 \mu\text{m}$  but grains of mixed complex structures are observed from  $50 \mu\text{m}$  to  $5 \mu\text{m}$ . In fact, different and smallest grains complex structures are observed only SEM image at  $50 \mu\text{m}$ .

### 3.4. UV-Vis spectra

We examined at room temperature UV-Vis absorption spectra of complex 1 in DCM solvent to get insights into the complexation of Cd(II) on the absorption property of ( $H_2L_{\text{pent}}^{\text{OMe}}$ ). In DCM, 1 exhibits ligand-based transition at  $353 \text{ nm}$  presumably due to  $\pi \rightarrow \pi^*$  or  $n \rightarrow \pi^*$  type of transitions [55,59]. Due to  $d^{10}$  electronic configuration of Cd(II) metal ion, no metal centric d-d broad absorption band was expected in the UV-Vis spectra (Fig. S2).

### 3.5. X-ray powder diffraction

The crystalline phase purity of azido-bridged  $\text{Cd}_2$ -nuclear metal complex was confirmed by X-ray powder diffraction pattern. X-ray powder diffraction patterns for 1 was experimentally recorded after considering (low theta scan  $2\theta$ ) from  $4^{\circ}$  to  $50^{\circ}$ . From Fig. S5, it was clearly (experimental) observed that most of the major peak positions of the bulk solid samples agree very well with the patterns simulated from single X-ray crystal diffraction data (CIF for 1), generally obtained from CCDC Mercury software consisting that single crystals and bulk material for 1 are the same. It also further confirms phase purity of the bulk crystal samples of  $\text{Cd}_2$ -nuclear metal complex.

## 4. X-ray crystal structure

### 4.1. Crystal structure of $[\text{Cd}_2(H_2L_{\text{pent}}^{\text{OMe}})(\mu_{1,1}\text{-N}_3)_2]_n$ (1)

The solid-state structure of azido-bridged Cd(II) coordination polymer has been confirmed by single X-ray crystal diffraction study. Complex 1 crystal structure parameters are shown in Table 1 and some important crystallographic parameters are summarized in Table S1. The molecule crystallizes in monoclinic space group  $C2/c$  with  $Z = 8$ . The asymmetric unit (Fig. 2) consists of one deprotonated Schiff base ligand [ $L_{\text{pent}}^{\text{OMe}}$ ] $^{2-}$ , two cadmium ions (Cd1 and Cd2) encapsulated in the two

**Table 2**  
Compartmental ligands coordinating ability with Cd(II) metal ion.

Compartmental ligands	Ligand pocket used	Cd(II)-azido CP/complexes	Ref
1. $[\text{N}, \text{N}'\text{-bis}(3\text{-methoxysalicylideneimino})\text{-1,3-diamino propane}]$ $[\text{H}_2\text{L}^{\text{OMe}}]$ [ $\text{N}, \text{N}'\text{-bis}(3\text{-ethoxysalicylideneimino})\text{-1,3-damino propane}$ ] $[\text{H}_2\text{L}^{\text{OEt}}]$	$\text{N}_2\text{O}_2$ and $\text{O}_2\text{O}_2$	$\mu_{1,3}$ & $\mu_{1,1}\text{-N}_3^-$ 1-D CP	35a
2. $[\text{N}, \text{N}'\text{-bis}(2\text{-hydroxy-3-methoxybenzylidene)})\text{-propane-1,2-diamine}$ $[\text{H}_2\text{L}^{\text{OMe}}]$ $\text{N}, \text{N}'\text{-bis}(2\text{-hydroxy-3-methoxybenzylidene)})\text{-propane-1,2-diamine}$ $[\text{H}_2\text{L}^{\text{OEt}}]$	$\text{N}_2\text{O}_2$ and $\text{O}_2\text{O}_2$	$\mu_{1,3}$ & $\mu_{1,1}\text{-N}_3^-$ 1-D CP $\mu_{1,1}\text{-N}_3^-$ discrete	35b
3. $\text{N}, \text{N}'\text{-bis}(3\text{-methoxysalicylaldimine})\text{-1,3-diaminopentane}$ $[\text{H}_2\text{L}_{\text{pent}}^{\text{OMe}}]$	$\text{N}_2\text{O}_2$ and $\text{O}_2\text{O}_2$ . Also O atom in -OMe group	$\mu_{1,1}\text{-N}_3^-$ 1-D CP	This work

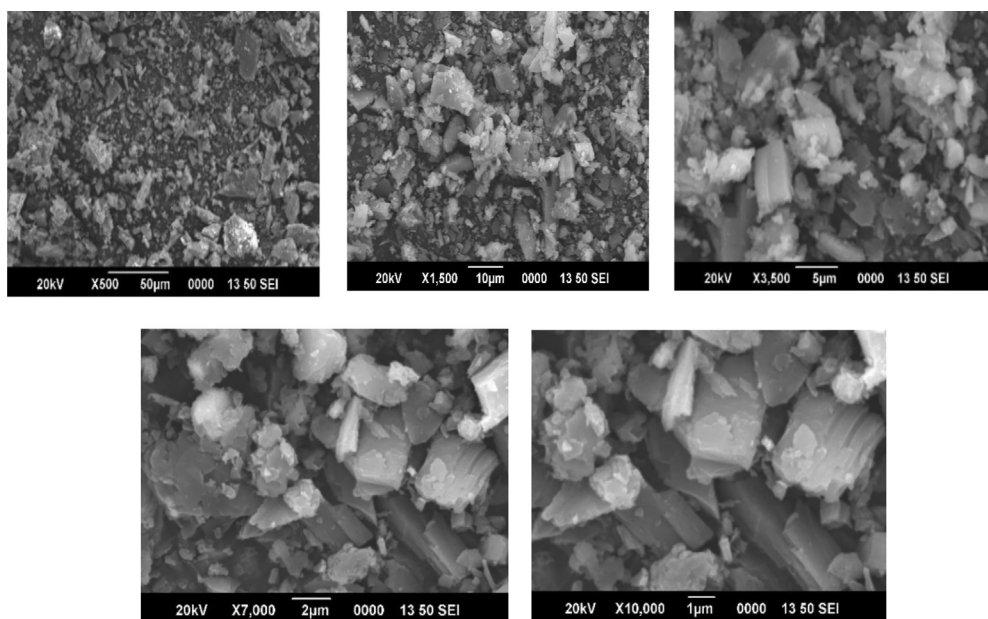


Fig. 1. SEM images of complex 1.

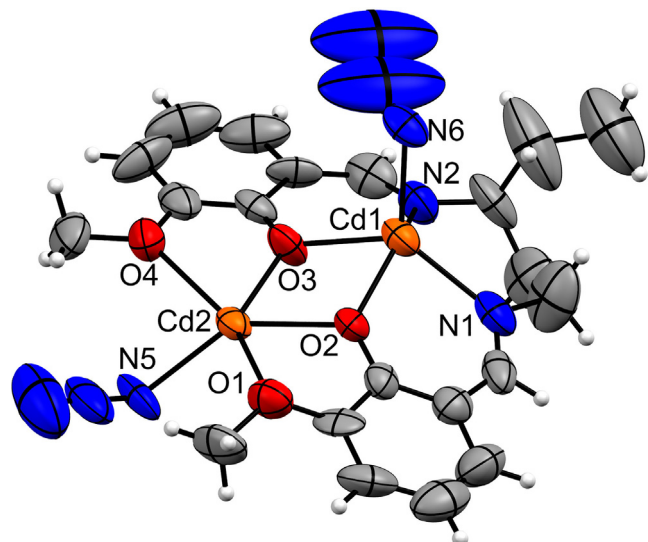


Fig. 2. Perspective view of asymmetric unit of complex 1.

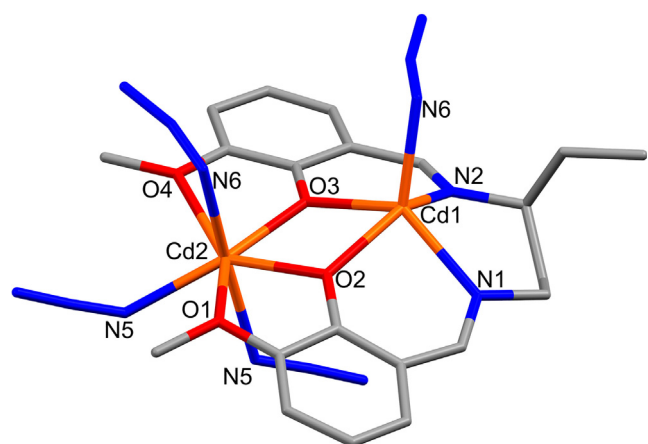


Fig. 3. Complete geometry of complex 1.

ligand pockets, and two small-sized azide ions coordinated to Cd1 and Cd2 metal. Therefore, single crystal structure divulges two different geometrical environment of cadmium metal centres. Structural environment of two cadmium metal centres were calculated from Addison parameter Tau ( $r$ ), ( $r = |\beta - \alpha|/60^\circ$  where  $\beta, \alpha$  are the two largest angles around cadmium metal atom;  $r = 0$  for a perfect square pyramidal and 1 for a perfect trigonal bipyramidal geometry) [60]. The Cd1 is coordinated to two deprotonated Schiff base ligand [ $L_{\text{pent}}^{\text{OMe}}\right]^{2-}$  phenolate oxygens (O2 and O3), two imine nitrogens (N1 and N2), and one azide nitrogen (N6). The N1, N2, O2, and O3 occupied equatorial positions and N6 occupied the apical position. As a result, the Cd1 adopted distorted square pyramidal geometry [ $(r)$  value 0.31] (Fig. 3) [35] where Cd1 is shifted towards the axial position by 0.825 Å. The Cd2 is further coordinated to two phenolate oxygen (O2 and O3), two methoxy oxygens (O1 and O4) in OMe group, three nitrogen atoms from three azide co-ligands. The Cd2 adopted distorted pentagonal bipyramidal (PBP) geometry [ $(r)$  value 0.09] [60] (Fig. 3) where the basal plane is occupied by O1, O2, O3, O4, N5 atoms, and axial positions are occupied by N5<sup>a</sup> and N6 atoms. Herein, Cd2 is shifted toward the axial position by 0.337 Å. The displacement of Cd1 and Cd2 is anti in nature from the basal plane (Fig. 3). The phenolate oxygens O2 and O3 bridged Cd1 and Cd2 where distance is 3.531 Å and Cd1-O2/O3-Cd2 angle is 104.2°. The Cd-Cd bond distance is totally comparable with previously reported Cd(II)-CP [61]. The N6 atom of azide co-ligand coordinated to Cd1 is connecting Cd2 atom of another symmetry-related molecule and N5 atom of another azide co-ligand coordinated to Cd2 is connecting another Cd2 atom of another symmetry-related molecule. As a result, it generated a (one-dimensional)1-D chain (Fig. 4) through coordination along the c axis. Herein, the azide ion act as  $\mu_2$ -bridging nature and coordinated two cadmium metal centers. In the solid-state, 1-D chains are hydrogen bonded to form three-dimension (3-D) network (Fig. S6). The azide ion bridging modes in complex 1 has been compared with previously reported Cd(II)-azido Schiff base complexes (Table S5). Selected some important bond distances and angles are shown in Table 3.

#### 4.2. FMO analysis

Complex 1 is optimized in the gas phase at B3LYP/TZVP level of theory and the frontier orbital investigation reveal that HOMO has an energy of around −5.227 eV and LUMO is around −1.793 eV in energy

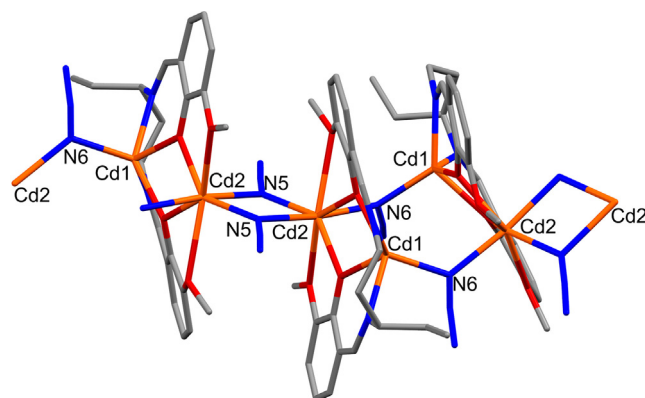


Fig. 4. 1-D chain through coordination in complex 1.

**Table 3**  
Selected some important Bond Distances ( $\text{\AA}$ ) and Bond angles ( $^{\circ}$ ) for complex 1.

Complex	Selected bond distances ( $\text{\AA}$ )	Value ( $\text{\AA}$ )	Selected bond angles ( $^{\circ}$ )	Value ( $^{\circ}$ )
1	Cd1-N1	2.26(1)	N1-Cd1-N2	89.5(4)
	Cd1-N2	2.27(1)	O2-Cd1-O3	75.9(2)
	Cd1-O2	2.210(7)	O2-Cd1-N6	119.9(3)
	Cd1-O3	2.241(8)	O3-Cd1-N6	102.8(3)
	Cd1-N6	2.218(9)	N1-Cd1-N6	125.5(4)
	Cd2-N6	2.290(8)	N2-Cd1-N6	94.8(4)
	Cd2-O1	2.693(8)	O1-Cd2-O2	62.3(2)
	Cd2-O2	2.265(7)	O2-Cd2-O3	75.0(2)
	Cd2-N5	2.221(1)	O3-Cd2-O4	64.9(2)
	Cd2-O3	2.234(7)	O1-Cd2-O4	151.6(2)
	Cd2-O4	2.587(6)	N5-Cd2-O4	103.8(3)
	N5-Cd2	2.367(9)	N6-Cd2-N5	106.4(3)
	N6-Cd2	2.29(8)	O1-Cd2-N6	76.3(3)
			O3-Cd2-N6	95.7(3)
			O4-Cd2-N6	84.1(3)
			O3-Cd2-N5	87.6(3)
			O4-Cd2-N5	83.0(3)
			O1-Cd2-N5	96.5(3)
			O2-Cd2-N5	86.9(3)

(Fig. 5). The calculation of energy difference between the frontier orbitals shows an energy gap of 3.434 eV which suggests that the molecule is low in chemical reactivity and is fairly stable. This is further probed by calculating global reactivity descriptors which predict a similar character for the molecule (Table S6). Further the frontier orbital composition analysis is carried out using the Mulliken method to investigate the character of these orbitals. As it is evident from Fig. 5, the HOMO of the cadmium complex is entirely concentrated on one of the azide co-ligands with a total contribution of *ca.* 96.77% ( $\pi$  type). Further a small contribution from one of the Cd metal centre is also seen (2.367%, d type). In case of LUMO, there is sharp contrast and as can be seen from the Fig. 5, it is entirely composed of the ( $\text{H}_2\text{L}_{\text{pent}}^{\text{OMe}}$ ) with the metal centre and azide co-ligands having no share. The azomethine group on either side of the metal centre has the highest contribution with a total of 50.62% ( $\pi^*$  type). This is followed by benzenoid type rings on both the sides of the ligand with a total of 40.69% ( $\pi^*$  type) contribution.

#### 4.3. Electrostatic potential analysis

MEP analysis is important in that respect that it is related to the electron density and is a very useful descriptors to find out the sites of electrophilic and nucleophilic [62]. The electrostatic potential plots were drawn on electron density isosurface using the DFT optimised structures (Fig. 6). These plots display electrophilic (blue colored) and nucleophilic (red colored) areas in the molecular surface. Both the Cd

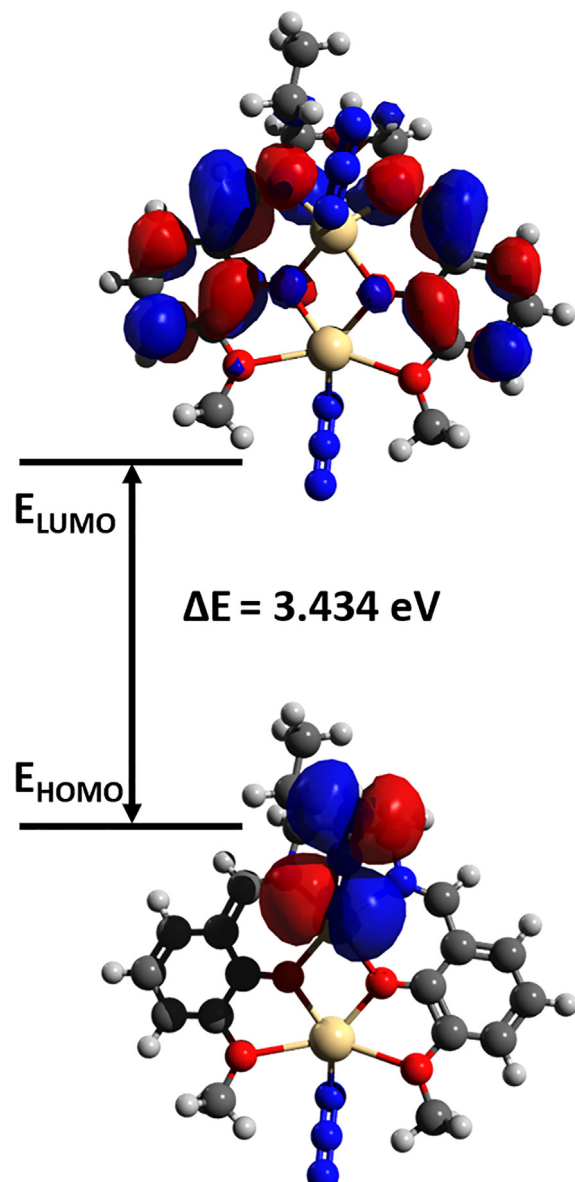
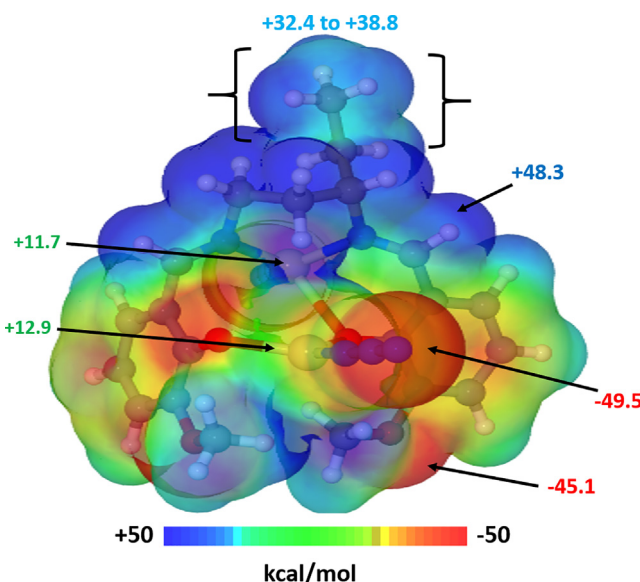


Fig. 5. Contour plot of frontier molecular orbitals of 1 (along with the energy gap).

(II) metal centres have a positive potential with the first one in the  $\text{N}_2\text{O}_2$  cavity having a slightly less value (+ 11.7 kcal/mol) than the one in the  $\text{O}_4$  cavity (+ 12.9 kcal/mol). This is well corroborated by the atomic charge calculations carried out using the Mulliken method where the former has a value of + 0.941 while the later has + 0.985. Both the azide co-ligands possess the highest negative potential with a value of - 49.5 kcal/mol and - 45.1 kcal/mol respectively. This along with the position of HOMO of the molecule suggests that the azide moiety dictates the chemical reactivity of the compound. When it comes to the highest positive potential, it is found near the azomethine hydrogen atom on both sides which is a common trait in these class of compounds [62]. It is also worth mentioning that the entire spacer diimine group exhibits a positive potential ranging from + 32.4 kcal/mol to + 38.8 kcal/mol.

#### 5. Solvatochromism

In order to evaluate solvent variation absorption and fluorescence spectra, we have analysed ‘solvatochromism’ where  $\text{Cd}_2$ -nuclear metal

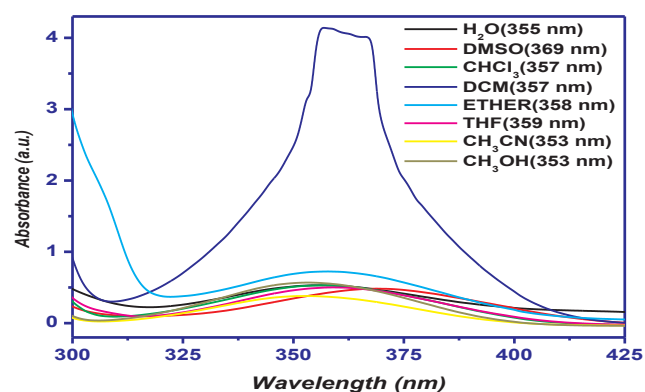


**Fig. 6.** Electrostatic potential plot mapped over the electron density isosurface of **1** (Computed at B3LYP/TZVP depicting the nucleophilic and electrophilic regions).

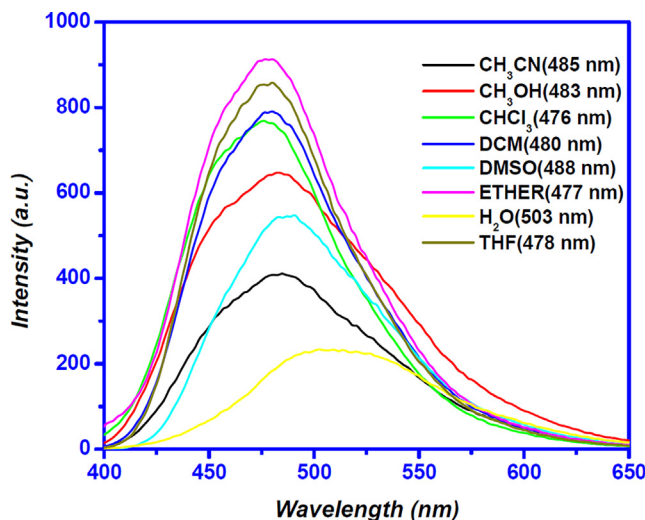
complex was dissolved in different variety of solvents. Dielectric constant and hydrogen bonding capacity are two important properties for all solvents, hence solvent variation greatly affected ground and excited state of the complex so that size of energy gap between them changes as polarity of solvent changes. Therefore, on passing from highly polar to less polar solvent absorption and fluorescence spectrum position, intensity and shape of the bands will be completely changed. It is worth to mention here that recently solvent dependent fluorescence emission observed for cadmium coordination polymer [63]. In addition, positive and negative ‘solvatochromism’ reflected red (for polarity of solvent if increased) and blue shift in the absorption and fluorescence emission spectrum. In our present situation, the absorption and fluorescence spectra for complex **1** was taken in solvents like DCM, DMSO,  $\text{CHCl}_3$ ,  $\text{H}_2\text{O}$ , Ether, THF,  $\text{CH}_3\text{CN}$ ,  $\text{CH}_3\text{OH}$  etc. It is noteworthy to mention here that on passing from less polar to highly polar solvent no remarkable changes of absorption spectrum band position except in DCM solvent it is more pronounced [63] whereas in highly protic solvent ( $\text{H}_2\text{O}$ ,  $\text{CH}_3\text{CN}$ , Ether,  $\text{CH}_3\text{OH}$ ) band positions are completely broad. In fact, solvent effects exposed large differences on the electronic fluorescence emission spectra between polar and non-polar solvents [63]. Herein we observed presence of highly protic solvent ( $\text{H}_2\text{O}$ ) fluorescence emission maxima at 503 nm (Fig. 8) and a red shift fluorescence emission increase of about ( $\lambda_{\text{em}}$  23 nm) but for other solvents these variations are less important. Therefore, increasing solvent polarity fluorescence emission maxima are largely red shifted compared to that of absorption band (Fig. 7). Thus, in **1** effect of solvent polarity on the fluorescence emission maxima was more pronounced than that on the absorption maxima [64]. The above fact indicates an increase of dipole moment of excited state compared to that of ground state. Further, on passing from less polar to highly polar solvent fluorescence spectral bands are more structurally organized compared to that of absorption spectra. Therefore, complex **1** is solvatochromic in nature [64].

## 6. Photoluminescence

$d^{10}$  metal ion complexes fluorescence properties are extremely important due to their versatile application in chemical sensors, in photochemistry and also in electroluminescent displays [65]. At room temperature photoluminescence property of **1** is monitored in DCM solvent followed by solid-state (Table 4). In DCM and solid-state upon



**Fig. 7.** Solvent-dependent absorption spectra for **1**.



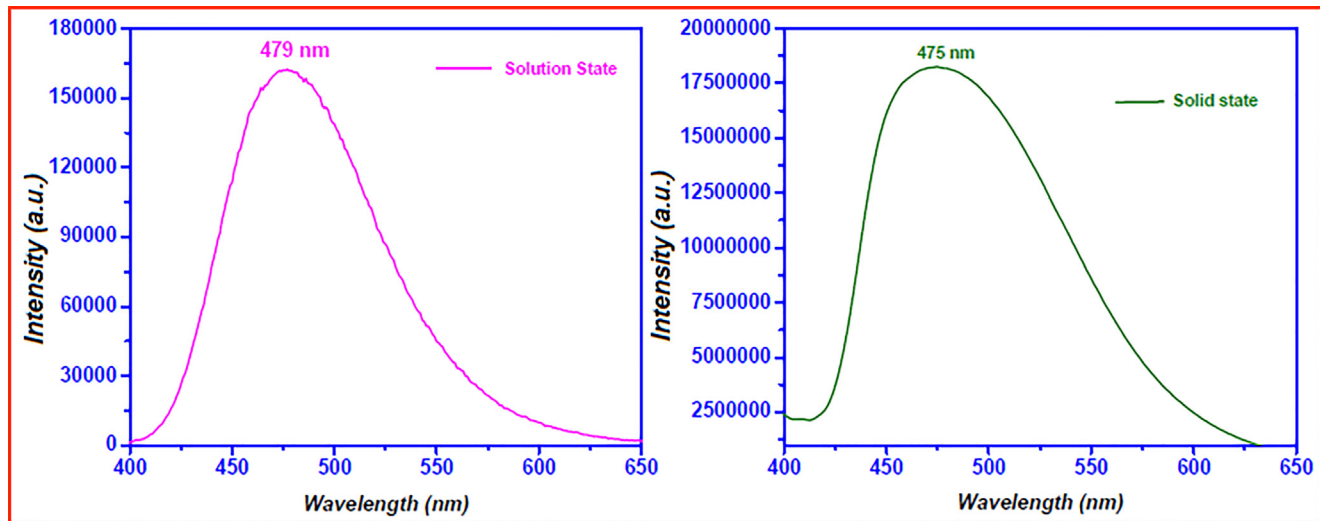
**Fig. 8.** Solvent-dependent fluorescence emission spectra for **1**.

photo excitation at wavelength 367 nm shows fluorescence maxima with the major emission peak near at 479 nm and 475 nm respectively (Fig. 9). Hence in DCM solvent complex **1** is fluorescent active over free Schiff base ligand [52]. The quenching of fluorescence behaviour under solid-state upon L-M complexation can be well explained with the help of magnetic perturbation, redox activity and electrons [66]. The higher fluorescence intensity of **1** over Schiff base is probably due to effective coordination of ligand donor centers to the cadmium metal ion, thereby increased the conformational rigidity of molecular complex via chelation enhanced fluorescence [CHEF] and subsequently loss of energy by radiation less thermal vibration. The filled  $d^{10}$  configuration of Cd(II) metal ion is difficult hard to oxidize or reduce. Such type fluorescence behaviour may be assigned due to the intra-ligand ( $\pi \rightarrow \pi^*$ ) transition or  $L \rightarrow M$  charge transfer [CHEF] [67–70] but for quenching ‘Chelation enhancement of Quenching effect’ (CHEQ) [71]. The emission nature of Schiff base and complex **1** is identical with previously reported salen-type ligands [6,52] and Cd(II)-Schiff base complexes (Table S7). The low quantum yield of ligand is due to fast Photoinduced electron transfer (PET) from ligand side to the conjugated phenolic moiety. Thus L-M complexation prevents PET process and thereby enhances quantum yield ( $\phi$ ) of complex **1** [72]. Complex exhibit good photoluminescence behaviour in DCM over solid-state since in DCM fluorescence behaviours are mainly ligand centered whereas in solid-state it is totally packing dependent [73]. To get a better understanding on emitting property, time-resolved fluorescence spectroscopic studies (excitation at 367 nm) in DCM and solid-state have been undertaken and lifetime decay profiles have been shown in Fig. S7-8. The decay profile in DCM will be best fitted to bi-exponential nature (with acceptable comparable

**Table 4**

Room temperature time-resolved photoluminescence decay.

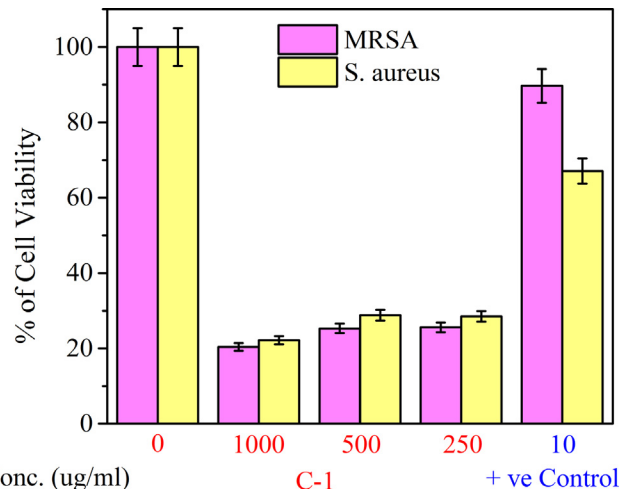
Compounds	$\lambda_{\text{ex}}$ (nm)	$\lambda_{\text{em}}$ (nm) (DCM)	$\lambda_{\text{em}}$ (nm) (Solid-state)	Quantum Yield ( $\phi$ )	Ref
<b>1</b> (H <sub>2</sub> Lpent <sup>OMe</sup> )	367 356	479 472	475 –	0.00664 0.0047	This work S2
Complex	$\lambda_{\text{ex}}[\text{nm}]$	$\lambda_{\text{em}}[\text{nm}]$	$\tau_1[\text{ns}]$	$\tau_2[\text{ns}]$	$\tau_3[\text{ns}]$
<b>1</b>	367	479	0.82(98%)	11.01(2.0%)	$<\tau> [\text{ns}]$
DCM solvent	367	472	4.51(24%)	–	$\chi^2$
Solid-state	367	472	10.6 (19%)	2.53	1.16
			0.56(57%)	7.74	1.11

**Fig. 9.** Fluorescence emission spectra for **1** in DCM solvent and solid-state.

$\chi^2$  values 1.16) whereas solid-state it is tuned to tri-exponential nature (with acceptable comparable  $\chi^2$  values 1.11) with lifetimes in the range (1.16–1.11 ns). However, in solid-state condition cadmium complex exhibit smaller lifetime than DCM and strictly there is a well definite trend observed in DCM solvent over solid-state (Table 4). Interestingly, in DCM, a regular lifetimes trend observed having two different decay times with maximum (98%) and minimum (2%) contribution in amplitude whereas in solid-state this trend is irregular maximum (57%), (24%) and minimum (19%) contribution in amplitude. Therefore, higher lifetime decay response one type of crystal packing and lower lifetime decay prefers another type of packing [73]. The calculated average lifetime value further divulges that importance of excited states stabilities of complex **1** is maximum in DCM than solid-state condition.

## 7. Antimicrobial activity

We have analysed concentration dependent antimicrobial activity of cadmium metal complex against two standard bacterial strains *Staphylococcus aureus* (ATCC 25923) and Methicillin-resistant *Staphylococcus aureus* (MRSA). Concentration dependent antimicrobial assay (Fig. 10) directly confirms that complex **1** has excellent antimicrobial efficiency against different microorganisms. 250  $\mu\text{g}/\text{ml}$  concentration of cadmium complex is sufficient to show the antimicrobial effect against *Staphylococcus aureus* (ATCC 25923) and Methicillin-resistant *Staphylococcus aureus* (MRSA). The cellular growth was inhibited by more than 75% at 250  $\mu\text{g}/\text{ml}$  concentration of complex **1** compared to control. Such antimicrobial efficiency of **1** was explained by joint concepts of Overtone's and Chelation theory [74]. Normally chelation enhances the delocalization of sigma electrons over the entire chelate ring of Schiff base ligand and reduces the polarity of cadmium metal ion to a large extent. Thereby easy penetration of complex **1** is facilitated into the lipid membrane and blocking the cadmium metal binding sites in enzymes of microorganisms [74]. A plausible

**Fig. 10.** Concentration dependent antimicrobial activity of complex **1** against *Staphylococcus aureus* (ATCC 25923) and Methicillin-resistant *Staphylococcus aureus* (MRSA).

mechanism is already published by A. D. Hashmi et al. in favour of the above mention discussion (Fig. 11) [74].

## 8. Conclusion

This paper carefully describes the synthesis and structural aspect of one new azido-bridged 1-D coordination polymer [ $\text{Cd}_2(\text{H}_2\text{Lpent}^{\text{OMe}})(\mu_{1,1}\text{-N}_3)_2$ ]<sub>n</sub> (**1**) derived from less explored bi-compartmental Schiff base ligand (H<sub>2</sub>Lpent<sup>OMe</sup>). The successful synthesis of CP was only achieved when Schiff base ligand properly utilizing their compartmental N<sub>2</sub>O<sub>2</sub><sup>-</sup> and O<sub>4</sub><sup>-</sup> donor sets. In the asymmetric unit, solid-state X-

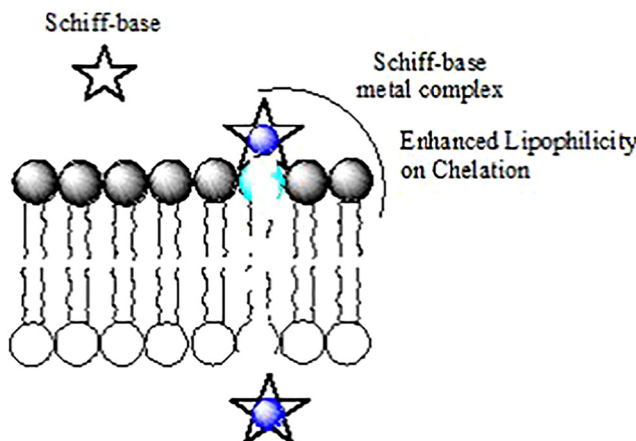


**Fig. 11.** Enhanced lipophilicity of cadmium metal complex on chelation favouring easy penetration of the complex into the bacterial lipid membrane.

ray crystal structure divulges distorted square pyramidal and distorted pentagonal bipyramidal geometry around cadmium metal centres. ORCA 3.0.3 and B3LYP level using TZVP basis set were successfully applied to explain FMO, MEP and global reactivity of the title complex. HOMO-LUMO energy gap suggests that chemical reactivity of cadmium metal complex is low but fairly stable. At room temperature steady state and time-resolved fluorescence spectroscopic measurements were conducted in DCM solvent and solid-state. Solvatochromism has been reported to explain solvent dependent absorption and fluorescence emission spectra. Fascinatingly, Cd(II) coordination polymer exhibit red shifted solvatochromism. Finally, concentration dependent anti-microbial activity was investigated against two standard bacterial strains (*Staphylococcus aureus* (ATCC 25923) and Methicillin-resistant *Staphylococcus aureus* (MRSA).

## Acknowledgements

This research work did not receive any specific grant from funding agencies in the public, commercial or not-profit sectors. Dr. Dipankar Mishra gratefully acknowledges the financial grant sanctioned by UGC, New Delhi, in his favour vide Minor Research Project (F.PSW-232/15-16(ERO). D. J. Majumdar is thankful to Prof. Dr. A. L. Spek (Emeritus), Utrecht University, Bijvoet Center for Biomolecular Research, Padualaan 8 3584 CH, Utrecht, The Netherlands, for providing fruitful suggestions in connection of A-Level alert resolution under X-ray crystallography.

## Appendix A. Supplementary data

Supplementary data to this article can be found online at <https://doi.org/10.1016/j.ica.2019.119069>.

## References

- [1] (a) S.R. Batten, S.M. Neville, D.R. Turner, Coordination polymers: design, analysis and application, Royal Society of Chemistry, Cambridge, 2009;
- (b) M.-C. Hong, L. Chen, Design and Construction of Coordination Polymers, John Wiley & Sons Inc, Hoboken, New Jersey, 2009;
- (c) G.R. Desiraju, J.J. Vittal, A. Ramanan, Crystal Engineering: A Text Book, World Scientific, Singapore, 2011;
- (d) M. Eddaoudi, D.F. Sava, J.F. Eubank, K. Adil, V. Guillerm, Chem. Soc. Rev. 44 (2015) 228–249;
- (e) C. Janiak, J.K. Vieth, New J. Chem. 34 (2010) 2366–2388;
- (f) S. Kitagawa, R. Kitaura, S.-I. Noro, Angew. Chem., Int. Ed. 43 (2004) 2334–2375;
- (g) H.-C. Zhou, J.R. Long, O.M. Yaghi, Chem. Rev. 112 (2012) 673–674 and all the articles in the special issue.
- (h) D. Sun, S. Yuan, H. Wang, H.-F. Lu, S.-Y. Feng, D.-F. Sun, Chem. Commun. 49 (2013) 6152–6154;
- (i) M.H. Mir, G.K. Tan, L.L. Koh, J.J. Vittal, Angew. Chem., Int. Ed. 49 (2010) 390–393;
- [2] B. Dutta, D. Das, J. Datta, A. Chandra, S. Jana, C. Sinha, P.P. Ray, M.H. Mir, Inorg. Chem. Front. (2019), <https://doi.org/10.1039/C9QI00162J>.
- [3] F.A. Mautner, F.R. Louka, J. Hofer, M. Spell, A. Lefevre, A.E. Guillebeau, S.S. Massoud, Cryst. Growth Des. 13 (2013) 4518–4525.
- [4] S.S. Massoud, F.R. Louka, Y.K. Obaid, R. Vicente, J. Ribas, R.C. Fischer, F.A. Mautner, Dalton Trans. 42 (2013) 3968–3978.
- [5] (a) F.A. Mautner, M. Koikawa, M. Mikuriya, E.H. Harrelson, J.G. Gautreaux, S.S. Massoud, Polyhedron 59 (2013) 17–22;
- (b) S.S. Massoud, F.R. Louka, T.L. Nguyen, M. Mikuriya, J.H. Albering, F.A. Mautner, Inorg. Chim. Acta 366 (2011) 394–398;
- (c) S.S. Massoud, F.A. Mautner, R. Vicente, A.A. Gallo, E. Ducasse, Eur. J. Inorg. Chem. (2007) 1091–1102;
- (d) S.S. Massoud, F.A. Mautner, Inorg. Chim. Acta 358 (2005) 3334–3340;
- (e) A. Escuer, M.F. Bardia, S.S. Massoud, F.A. Mautner, E. Penalba, X. Solans, New J. Chem. 28 (2004) 681–686.
- (f) F.A. Mautner, B. Sudy, A. Egger, E.M. Mautner, A. Escuer, R. Vicente, Inorg. Chem. Commun. 21 (2012) 4–7;
- (g) F.A. Mautner, B. Sudy, C. Berger, R.C. Fischer, R. Vicente, Polyhedron 42 (2012) 95–101;
- (h) F.A. Mautner, B. Sudy, R. Vicente, Inorg. Chim. Acta 378 (2011) 23–27
- [6] M. Maiti, S. Thakurta, D. Sadhukhan, G. Pilet, G.M. Rosair, A. Nonat, L.J. Charbonniere, S. Mitra, Polyhedron 65 (2013) 6–15.
- [7] (a) J. Boeckmann, C. Nather, Polyhedron 31 (2012) 587–595;
- (b) D. Maity, S. Chattopadhyay, A. Ghosh, M.G.B. Drew, G. Mukhopadhyay, Inorg. Chim. Acta 365 (2011) 25–31.
- [8] (a) G.A. van Albada, M.G. van der Horst, I. Mutikainen, U. Turpeinen, J. Reedijk, Inorg. Chim. Acta 376 (2011) 15–20;
- (b) A. Ray, G.M. Rosair, G. Pilet, B. Dede, C.J. Gomez-Garcia, S. Signorella, S. Bellu, S. Mitra, Inorg. Chim. Acta 375 (2011) 20–30;
- (c) P. Bhunia, D. Banerjee, P. Datta, P. Raghavaiah, A.M.Z. Slawin, J.D. Woollins, J. Ribas, C. Sinha, Eur. J. Inorg. Chem. (2010) 311–321;
- (d) X. Lin, J. Tao, R.-B. Huang, L.-S. Zheng, Inorg. Chem. Commun. 12 (2009) 154–156;
- (e) Z.G. Gu, Y. Song, J.L. Zuo, X.-Z. You, Inorg. Chem. 46 (2007) 9522–9524;
- (f) Z.-L. Chen, C.-F. Jiang, W.-H. Yan, F.-P. Liang, S.R. Batten, Inorg. Chem. 48 (2009) 4674–4684.
- [9] (a) M.-H. Zeng, Y.-L. Ahou, W.-X. Zhang, M. Du, H.-L. Sun, Cryst. Growth Des. 10 (2010) 2024;
- (b) M.A.M. Abu Youssef, A. Escuer, F.A. Mautner, L. Ohrstrom, Dalton Trans. (2008) 3553–3558;
- (c) M.A.M. Abu Youssef, F.A. Mautner, R. Vicente, Inorg. Chem. 46 (2007) 4654–4659.
- [10] D. Mandal, V. Bertolasi, J. Ribas-Arino, G. Aromi, D. Ray, Inorg. Chem. 47 (2008) 34653467.
- [11] S.-Q. Bai, E.-Q. Gao, Z. He, C.-J. Fang, C.-H. Yan, New J. Chem. 29 (2005) 935–941.
- [12] (a) T.C. Stamatatos, G.S. Papaefstathiou, L.R. MacGillivray, A. Escuer, R. Vicente, E. Ruiz, S.P. Perlepes, Inorg. Chem. 46 (2007) 8843–8850;
- (b) A. Escuer, G. Aromi, Eur. J. Inorg. Chem. (2006) 4721;
- (c) G.S. Papaefstathiou, S.P. Perlepes, A. Escuer, R. Vicente, M. Font-Bardia, X. Solans, Angew. Chem., Int. Ed. 40 (2001) 884–886;
- (d) G.S. Papaefstathiou, A. Escuer, R. Vicente, M. Font-Bardia, X. Solans, S.P. Perlepes, Chem. Commun. (2001) 2414–2415.
- [13] C. Adhikary, S. Koner, Coord. Chem. Rev. 254 (2010) 2933–2958.
- [14] M.-Z. Zeng, Y.-L. Zhou, W.-X. Zhang, M. Du, H.-L. Sun, Cryst. Growth Des. 10 (2010) 20–24.
- [15] G.A. van Albada, I. Mutikanian, O. Roubeau, J. Reedijk, J. Mol. Struct. 1036 (2013) 252–256.
- [16] M. Monfort, I. Resino, J. Ribas, X. Solans, M.F. Bardia, New J. Chem. 25 (2001) 1577.
- [17] M. Monfort, I. Resino, J. Ribas, X. Solans, H. Stoeckli-Evans, Angew. Chem., Int. Ed. 39 (2000) 191–193.
- [18] J. Boonmak, M. Nakano, N. Chaichit, C. Pakawatchai, Y. Youngme, Inorg. Chem. 50 (2011) 7324–7333.
- [19] (a) X.-T. Wang, X.-H. Wang, Z.-M. Wang, S. Gao, Inorg. Chem. 48 (2009) 1301–1308;
- (b) J.-P. Zhao, B.-W. Hu, E.C. Sanudo, Q. Yang, Y.-F. Zeng, X.-H. Bu, Inorg. Chem. 48 (2009) 2482–2489.
- [20] (a) A.N. Georgopoulou, C.R. Raptopoulou, V. Psycharis, R. Ballesteros, B. Abarca, A.K. Boudlais, Inorg. Chem. 48 (2009) 3167–3176;
- (b) L.-F. Zhang, M.-M. Yu, Z.-H. Ni, A.-L. Cui, H.-Z. Kou, J. Mol. Struct. 1006 (2011) 629–634.
- [21] C.-B. Tian, Z.-H. Li, J.-D. Lin, S.-T. Wu, S.-W. Du, P. Lin, Eur. J. Inorg. Chem. (2010) 427–437.
- [22] M.A.S. Goher, F.A. Mautner, K. Gatterer, M.A.M. Abu-Youssef, A.M.A. Badr, B. Sudin, C. Gspan, J. Mol. Struct. 867 (2008) 199–205.
- [23] A.N. Georgopoulou, C.R. Raptopoulou, V. Psycharis, R. Ballesteros, B. Abarca, A.K. Boudlais, Inorg. Chem. 48 (2009) 3167.
- [24] (a) L.B. Lopes, C.C. Correa, G.P. Guedes, M.G.F. Vaz, R. Diniz, F.C. Machado, Polyhedron 50 (2013) 16–21;
- (b) S.S. Massoud, A.E. Guillebeau, H.T. Luong, R. Vicente, J.H. Albering, R.C. Fischer, F.A. Mautner, Inorg. Chim. Acta 362 (2009) 4073.
- [25] (a) F.A. Mautner, J.H. Albering, R. Vicente, C. AndrePont, J.G. Gautreaux, A.A. Gallo, S.S. Massoud, Polyhedron 54 (2013) 158–163;
- (b) S.S. Massoud, F.A. Mautner, F.R. Louka, S. Demeshko, S. Dechert, F. Meyer,

- Polyhedron 30 (2011) 2690.
- [26] (a) L. Li, B.-B. Guo, J. Zhang, G. Li, Inorg. Chem. Commun. 36 (2013) 86–89;  
 (b) T. Ma, J. Zhang, X. Jing, Q. Feng, B. Zheng, Y. Yu, Q. Huo, Y. Liu, Inorg. Chem. Commun. 20 (2012) 201–204;  
 (c) F.A. Mautner, J.H. Albering, M. Corbella, F.R. Louka, S.S. Massoud, Inorg. Chim. Acta. 14 (2011) 702–705.
- [27] (a) F.A. Mautner, F.R. Louka, S.S. Massoud, J. Mol. Struct. 921 (2009) 333–340;  
 (b) F.R. Louka, F.A. Mautner, R. Vicente, S.S. Massoud, Inorg. Chem. Commun. 11 (2008) 438–441.
- [28] (a) S.S. Massoud, K.J. Pujol, F.A. Mautner, S. Demeshko, S. Dechert, F. Meyer, Inorg. Chem. Commun. 30 (2013) 65–68;  
 (b) F.R. Louka, A.D. Stewart, E. Regel, F.A. Mautner, S. Demeshko, F. Meyer, S.S. Massoud, Inorg. Chem. Commun. 22 (2012) 60–64;  
 (c) T. LeGuet, F.A. Mautner, S. Demeshko, F. Meyer, R.S. Perkins, S.S. Massoud, Inorg. Chem. Commun. 12 (2009) 321–324;  
 (d) R. Vicente, E. Ruiz, J. Cano, S.S. Massoud, F.A. Mautner, Inorg. Chem. 47 (2008) 4648–4655;  
 (e) S.S. Massoud, F.A. Mautner, R. Vicente, F.R. Louka, Eur. J. Inorg. Chem. (2008) 3709;  
 (f) J. Carranza, J. Sletten, F. Lloret, M. Julve, Inorg. Chim. Acta. 371 (2011) 13–19.
- [29] (a) S.S. Massoud, R. Vicente, P.R. Fontenot, A.A. Gallo, M. Mikuriya, J.H. Albering, F.A. Mautner, Polyhedron 46 (2012) 66–73;  
 (b) E.E.B. de Paula, L.C. Visentin, M.I. Yoshida, L.F.C. De Oliveira, F.C. Machado, Polyhedron 30 (2011) 213–220.
- [30] A. Escuer, G. Aromi, Eur. J. Inorg. Chem. (2006) 4721–4736.
- [31] S. Roy, S. Bhattacharya, S.S. Mohanta, ChemistrySelect 2 (2017) 11091–11099.
- [32] H. Deng, C.J. Donan, H. Furukawa, R.B. Ferriera, J. Towne, C.B. Knobler, B. Wang, O.M. Yaghi, Science 327 (2010) 846–850.
- [33] F. Geng, R. Ma, T. Sasaki, Acc. Chem. Res. 43 (2010) 1177–1185.
- [34] Y. Hasegawa, T. Nakagawa, T. Kawai, Coord. Chem. Rev. 254 (2010) 2643–2651.
- [35] (a) D.J. Majumdar, M.S. Surendra Babu, S. Das, C. Mohapatra, J.K. Biswas, M. Mondal, ChemistrySelect 2 (2017) 4811–4822;  
 (b) D.J. Majumdar, S. Dey, S.S. Sreekumar, S. Das, D. Das, J.K. Biswas, M. Mondal, P. Shukla, T. Pal, K. Bankura, D. Mishra, J. Mol. Struct. 1179 (2019) 694–708;  
 (c) D.J. Majumdar, S. Das, J.K. Biswas, M. Mondal, J. Mol. Struct. 1134 (2017) 617–624.
- [36] (a) D.J. Majumdar, M.S. Surendra Babu, S. Das, J.K. Biswas, M. Mondal, J. Mol. Struct. 1138 (2017) 161–171;  
 (b) D.J. Majumdar, J.K. Biswas, M. Mondal, M.S. Surendra Babu, R.K. Metre, S. Das, K. Bankura, D. Mishra, J. Mol. Struct. 1155 (2018) 745–757;  
 (c) D.J. Majumdar, J.K. Biswas, M. Mondal, M.S. Surendra Babu, S. Das, R.K. Metre, S.S. SreeKumar, K. Bankura, D. Mishra, ChemistrySelect 3 (2018) 2912–2925;  
 (d) D.J. Majumdar, S. Dey, S.S. Sreekumar, S. Das, D. Das, R.K. Metre, K. Bankura, D. Mishra, ChemistrySelect 3 (2018) 12371–12382;  
 (e) doi: 10.1016/j.jica.2019.02.022.  
 (f) https://doi.org/10.1016/j.jica.2019.04.041.
- [37] (a) H. Strasdeit, W. Saak, S. Pohl, W.L. Driessen, J. Reedijk, Inorg. Chem. 27 (1988) 1557;  
 (b) A. Domenicano, L. Torelli, A. Vaciago, L. Zambonelli, J. Chem. Soc. A (1968) 1351–1361;  
 (c) B.F. Hoskins, B.P. Kelly, Inorg. Nucl. Chem. Lett. 8 (1972) 875–878;  
 (d) E.F. Epstein, I. Bernal, J. Chem. Soc. A (1971) 3628–3631;  
 (e) D. Sadhukhan, A. Ray, G. Rosair, L. Charbonniere, S. Mitra, Bull. Chem. Soc. Jpn. 2 (2011) 211–217.
- [38] D. Bose, J. Banerjee, S.H. Rahaman, G. Mostafa, H.-K. Fun, R.D.B. Walsh, M.J. Zawortko, B.K. Ghosh, Polyhedron 23 (2004) 2045–2053.
- [39] B. Valeur, Molecular Fluorescence, Principles and Applications, fifth ed. Wiley-VCH, Weinheim, 161 (2009).
- [40] G.M. Sheldrick, SADABS, a software for empirical absorption correction, Ver. 2.05, University of Göttingen: Göttingen, Germany, 2002.
- [41] SMART & SAINT Software Reference manuals, Version 6.45; Bruker Analytical X-ray Systems Inc.: Madison, WI, 2003.
- [42] SHELXTL Reference Manual, Ver. 6.1; Bruker Analytical X-ray Systems, Inc.: Madison, WI, 2000.
- [43] G.M. Sheldrick, SHELXTL a software for empirical absorption correction Ver. 6.12; Bruker AXS Inc.: WI. Madison, 2001.
- [44] O.V. Dolomanov, L.J. Bourhis, R.J. Gildea, J.A.K. Howard, H. Puschmann, OLEX2, J. Appl. Crystallogr. 42 (2009) 339.
- [45] K. Bradenburg, Diamond, Ver. 3.1eM; Crystal Impact GbR: Bonn, Germany, 2005.
- [46] (a) F. Neese, WIREs Comput. Mol. Sci. 2 (2012) 73–78;  
 (b) F. Neese, Orca. An ab Initio, Density Functional and Semiempirical Program Package version, 2009.
- [47] (a) A.D. Becke, J. Chem. Phys. 98 (1993) 1372;
- (b) C. Lee, W. Yang, Phys. Rev. B. 37 (1988) 785.
- [48] A. Schaefer, H. Horn, R. Ahlrichs, J. Chem. Phys. 97 (1992) 2571.
- [49] F. Weigend, R. Ahlrichs, Phys. Chem. Chem. Phys. 7 (2005) 3297.
- [50] M.D. Hanwell, D.E. Curtiss, D.C. Lonie, T. Vandermeersch, E. Zurek, G.R. Hutchison, J. Cheminform. (2012), <https://doi.org/10.1186/1758-2946-4-17>.
- [51] (a) T. Lu, F. Chen J. Comp. Chem. 33 (2012) 580–592; (b) <https://doi.org/10.1371/journal.pone.0137614>.
- [52] M. Maiti, D. Sadhukhan, S. Thakuta, S. Roy, G. Pilet, R.J. Butcher, L.J. Charbonniere, S. Mitra, Inorg. Chem. 51 (2012) 12176–12187.
- [53] C. Maxim, T.D. Pasatoiu, V.Ch. Kravtsov, S. Shova, C.A. Muryn, R.E.P. Winpenny, F. Tuna, M. Andruh, Inorg. Chim. Acta. 361 (2008) 3903–3911.
- [54] D.R. Turner, A.S.R. Chesman, K.S. Murray, G.B. Deacon, S.R. Batten, Chem. Commun. 47 (2011) 10189–10210.
- [55] A.B. Lever, Inorganic Spectroscopy, second ed., Elsevier, New York, 1984.
- [56] (a) J.E. Pate, P.K. Ross, T.J. Thamann, C.A. Reed, K.D. Karlin, T.N. Sorrell, E.I. Solomon, J. Am. Chem. Soc. 111 (1989) 5198–5209;  
 (b) D.A. Dows, E. Whittle, G.C. Pimentel, J. Chem. Phys. 23 (1955) 1475.
- [57] W.K. Dong, Y.X. Sun, C.Y. Zhao, X.Y. Dong, L. Xu, Polyhedron 29 (2010) 2087–2097.
- [58] (a) <https://doi.org/10.1080/24701556.2019.1603160>; (b) <https://doi.org/10.1016/j.arabjc.2010.05.001>.
- [59] J. Garcia, L.E. Sole, D. Jaque Bausa, An Introduction to the Optical Spectroscopy of Inorganic Solids, John Wiley & Sons, New York, 2005.
- [60] (a) A.W. Addison, T.N. Rao, J. Reedijk, J.V. Rijn, G.C. Verschoor, J. Chem. Soc., Dalton Trans. (1984) 1349–1356; (b) DOI: 10.1039/C4CE02140A.
- [61] DOI:10.1039/c2ce26525g.
- [62] (a) H. Wang, T. Lan, X. Zhang, D. Zhang, C. Bi, Y. Fan, J. Inorg. Biochem. 165 (2016) 18–24;  
 (b) N. Okulik, A.H. Jubert, Internet electron, J. Mol. Des. 4 (2005) 17–30;  
 (c) S.S. Sreejith, N. Mohan, M.R.P. Kurup, Polyhedron 135 (2017) 278–295.
- [63] (a) <https://doi.org/10.1002/aoc.5056>. (b) <https://doi.org/10.1039/c4cc00805g>;  
 (c) <https://doi.org/10.1021/jo200231k>; (d) <https://doi.org/10.1039/C4P04963B>.
- [64] <https://doi.org/10.1016/j.bmcl.2012.11.003>.
- [65] <https://doi.org/10.1002/slct.201803542>.
- [66] (a) A.W. Varnes, R.B. Dadson, E.L. Wehrly, J. Am. Chem. Soc. 94 (1972) 946–950;  
 (b) J.A. Kemlo, T.M. Sheperd, Chem. Phys. Lett. 47 (1977) 158–162.
- [67] J.R. Lakowicz, Topics in Fluorescence Spectroscopy, Plenum Press, New York, 1994.
- [68] S. Ray, S. Konar, A. Jana, S. Patra, S. Chatterjee, J.A. Golen, A.L. Rheingold, S. Mandal, S.K. Kar, Polyhedron 33 (2012) 82–89.
- [69] W. Gan, S.B. Jones, J.H. Reibenspies, R.D. Hancock, Inorg. Chim. Acta. 358 (2005) 3958–3966.
- [70] (a) Y. Li, L. Shi, L.-X. Qin, L.-L. Qu, C. Jing, M. Lan, T.D. James, Y.-T. Long, Chem. Commun. 47 (2011) 4361–4363;  
 (b) P. Ciesla, P. Kocot, P. Mytych, Z. Stasicka, J. Mol. Catal. A. Chem. 224 (2004) 17–33;  
 (c) A. Jr, Valem, Coord. Chem. Rev. 200 (2000) 933–978;  
 (d) A.P. de Silva, D.P. Fox, A.J. Huxley, T.S. Moody, Coord. Chem. Rev. 205 (2000) 41–57;  
 (e) D.-W. Fu, H.-L. Cai, S.-H. Li, Q. Ye, W. Zhang, Y. Zhang, X.-Y. Chen, G. Giovannetti, M. Capone, J. Li, R.-G. Xiong, Science 339 (2013) 425–428;  
 (f) D.-W. Fu, W. Zhang, H.-L. Cai, Y. Zhang, J.-Z. Ge, R.-G. Xiong, S.D. Huang, J. Am. Chem. Soc. 133 (2011) 12780–12786;  
 (g) D.-W. Fu, W. Zhang, H.-L. Cai, J.-Z. Ge, Y. Zhang, R.-G. Xiong, Adv. Mater. 23 (2011) 5658–5662;  
 (h) D.-W. Fu, H.-L. Cai, S.-H. Li, Q. Ye, L. Zhou, Y. Zhang, F. Deng, R.-G. Xiong, Phys. Rev. Lett. 110 (2013) 257601;  
 (i) W.-Y. Zhang, Y.-Y. Tang, P.-F. Li, P.-P. Shi, W.-Q. Liao, D.-W. Fu, H.-Y. Ye, Y. Zhang, R.-G. Xiong, J. Am. Chem. Soc. 139 (2017) 10897–10902.
- [71] M. Formica, V. Fusi, L. Giorgi, M. McHeloni, Coord. Chem. Rev. 356 (2012) 170–192.
- [72] (a) Z. Wang, J. Wang, J. Li, M. Feng, G. Zou, X. Huang, Chem. Commun. 51 (2015) 3094–3097;  
 (b) K. Takahashi, Y. Hasegawa, R. Sakamoto, M. Nishikawa, S. Kume, E. Nishibori, H. Nishihara, Inorg. Chem. 51 (2012) 5188–5198;  
 (c) J. Kanady, E. Tsui, M. Day, T.A. Agapie, Science 333 (2011) 733–736;  
 (d) P. Ghosh, P.K. Bharadwaj, J. Roy, S. Ghosh, J. Am. Chem. Soc. 119 (1997) 11903–11911;  
 (e) P. Ghosh, P.K. Bharadwaj, S. Mondal, S. Ghosh, J. Am. Chem. Soc. 118 (1996) 1553–1554.
- [73] N. Dwivedi, S.S. Sunkari, A. Verma, S. Saha, Cryst. Growth Des. 18 (9) (2018) 5628–5637.
- [74] (a) M.A. Malik, O.A. Dar, P. Gull, M.Y. Wani, A.D. Hashmi, Med. Chem. Commun. 9 (2018) 409–436;  
 (b) A.P. Mishra, R. Mishra, R. Jain, S. Gupta, Mycobiology 40 (2012) 20–26.